An acoustically matched traveling-wave thermoacoustic generator achieving 750 W electric power

Kai Wang[a,b], Daming Sun[a,b,*], Jie Zhang[a,b], Ya Xu[a,b], Kai Luo[a,b], Ning Zhang[a,b], Jiang Zou[a,b], Limin Qiu[a,b]

[a] *Institute of Refrigeration and Cryogenics, Zhejiang University, Hangzhou 310027, PR China;*

[b] *Key Laboratory of Refrigeration and Cryogenic Technology of Zhejiang University, PR China*

Abstract

Traveling-wave thermoacoustic electric generator (TWTEG) is promising in efficiently converting the heat of fuel combustion, solar energy, industrial waste heat, etc. into electricity with a very scalable power output. Based on the decoupling method and theoretical analysis, the acoustic impedance requirements of the traveling-wave thermoacoustic engine (TWTE) and linear alternators (LAs) to reach an efficient and powerful operation state were studied quantitatively. A 1 kW level traveling-wave thermoacoustic electric generator was then built for experimental study. Good matching conditions of acoustic impedances were then experimentally demonstrated by modulating the working frequency, load resistance, and electric reactance of the thermoacoustic electric generator, which agreed well with the theoretical analysis. A maximum electric power output of 750.4 W and a highest thermal-to-electric efficiency of 0.163 have been achieved by the acoustically matched thermoacoustic electric generator with helium of 3.16 MPa as the working gas. This work would be instructive for the acoustic matching and designs of high-performance thermoacoustic electric generation systems.

Keywords: thermoacoustic; electric generator; acoustic impedance; matching

[*] Corresponding authors. Tel/Fax: +86-571-87952769 (Daming Sun)
E-mail address: wangkai7089@gmail.com (K. Wang), sundaming@zju.edu.cn (Daming Sun)

1. Introduction

The continuous exhaustion of conventional energy resources and their environmental impacts have intrigued an increasing interest in the utilization of solar energy and thermal energy existing in industrial waste throughout the world. Various types of energy harvesting technologies and devices have been developed in the past decades, such as those based on photovoltaic effect [1], thermomagnetic effect [2], piezoelectric effect [3], and thermoelectric effect [4] etc. Thermoacoustic effect, which was first theoretically explained by Rayleigh [5] in 1878 and later efficiently utilized to convert thermal energy into acoustic power by Swift et. al. in 1999 [6], is among the most attractive and promising energy conversion phenomena.

When oscillating gas is exposed to a large temperature gradient along a porous medium, thermal energy can be converted into acoustic power through thermoacoustic effect. The appropriate acoustic field for energy conversion is typically formed by a resonant acoustic network system simply consisting of acoustic pipes. Due to the unique features of simple structure, high reliability, and intrinsically high efficiency, dozens of thermoacoustic energy conversion systems [7-15] have been manufactured in recent years. For practical applications, the acoustic power generated by thermoacoustic engines (TEs) has to be converted into electricity via acoustoelectric converters, such as linear alternators (LAs) [16-20], loudspeakers [13, 21], piezoelectric transducers [22], magnetohydrodynamic generator [23], and ferrite core coil with variable inductance [24], etc. The power outputs of the latter four thermoacoustic electric generation systems are typically in the range from several milliwatts to tens of watts, and may supply electricity for low-power electrical elements. TWTEGs, which are composed of a traveling-wave thermoacoustic engine (TWTE) and LAs, are very promising in higher power solar energy exploitation, waste heat recovery, and combined heat and power systems, etc. For the potential to achieve large power output and high efficiency simultaneously, TWTE has attracted considerable attention recently [16-20]. The first TWTEG was developed by Backhaus et al. for electricity generation aboard spacecraft in 2004 [25, 26]. It was capable of providing an electric power of 39 W. Similar systems were later built by Sunpower [27] and Wang et al. [20]. Wu et al. built several TWTEGs with various configurations recently, including a TWTEG with a resonator [17, 28], a TWTEG with double-acting alternators [18], and a TWTEG with resonant tubes [29]. The power outputs ranged from hundred watts to kilowatts, showing a good application prospective.

In the small-scale TWTEG developed by Backhaus et al., the long gas resonator, which acts as an acoustic inertance for the acoustically capacitive thermoacoustic torus in a TWTE, was totally replaced by a pair of LAs [25, 26]. LAs were thus operated at an inertance state, i.e. a phase difference between pressure and velocity of around 80°~90°. To meet the requirement of the large volume flow rate out of thermoacoustic torus, the piston diameters of LAs were designed to reach a large swept volume of 21 cm^3, which is comparable to the size of the torus. However, it would be a big challenge for LAs to be individually coupled with a traveling-wave thermoacoustic torus with an output capacity of ~kilo watts, due to the conflict between the large volume flow rate required and the limited swept volume of LAs. For example, the peak volume flow rate of TWTE built by Backhaus and Swift [6] is as high as 0.3 m^3/s, which is far beyond the limits of most available LAs. Gas resonator, which is usually a long

inertance tube together with a reservoir in a TWTE, is capable of providing a stable standing-wave acoustic field with a large volume flow rate at almost a constant frequency. Therefore, it is more feasible to couple LAs together with a gas resonator to a thermoacoustic torus so as to bypass the large volume flow without pushing LAs out of the limit in larger scale systems. Up to now, several TWTEGs of this type have been built and studied. In 2011, a TWTEG with a maximum electric power of 481.0 W and a highest thermal-to-electric efficiency of 15.03% was reported by Luo et al. [17]. Later, they built a prototype of 1 kW TWTEG [28]. In the experiments, 4.5% argon-helium mixture at 4.0 MPa was used as the working gas. However, the achieved acoustic impedance of the LA did not meet the requirements for the efficient operation of the TWTE. The effects of some important parameters, such as electric load resistance and electric capacitance, on the acoustic matching were not studied yet.

In a power circuit, the impedance of an electric load should be matched to the circuit to get optimal power output and high efficiency simultaneously. Similar to the electric load in the power circuit, LAs and the gas resonator are two acoustic loads to the thermoacoustic torus—the acoustic power source. Therefore, the characteristics of the acoustic impedances of them are very important to electric power generation and the control of acoustic power dissipations. For example, a real gas resonator always has an unavoidable resistance impedance apart from the dominant inertance one, and will cause considerable acoustic power losses if the acoustic impedance distribution between the gas resonator and the LA is not designed elaborately. However, the acoustic coupling mechanism between LAs and TEs and the effective approaches to acoustically match them have not yet been clearly addressed from the perspective of acoustic impedance in previous studies. Large space is still left for further improving the performance of TWTEGs. In 2012, we experimentally studied the effects of acoustic transfer line, electric loads and resonance characteristics of a TWTEG [16, 30]. By making the system both electrical and mechanical resonant, a maximum electric power of 345.3 W and a highest thermal-to-electric efficiency of 12.33% were achieved. Recently, the system achieved an electric power of 473.6 W with a maximum efficiency of 14.5% after further optimizations [19]. In the present study, the acoustic impedance modulations and matching for a TWTEG capable of generating 750 W electric power are presented in detail. The acoustic impedance requirements of the TWTE and LAs to reach efficient and powerful operation states are firstly studied by decoupling the whole TWTEG system. Experiments are then conducted to verify the theoretical analysis and numerical simulations, and characterize the acoustic matching working condition. The working mechanisms are analyzed from the aspect of the acoustic impedance. Further approaches for the improvements and the predicted performances are finally presented.

2. Theoretical analysis

2.1 Experimental apparatus

A TWTEG consisting of a TWTE and a pair of LAs and its corresponding equivalent electric circuit network are illustrated in FIG. 1. The TWTE consists of a resonator, an inertance tube, a compliance tube, a main ambient heat exchanger, a regenerator, a hot heat exchanger, a thermal buffer tube and a second ambient heat exchanger. The harmful Gedeon streaming flowing around the loop is totally eliminated by a silica membrane above the main ambient heat exchanger. The regenerator is

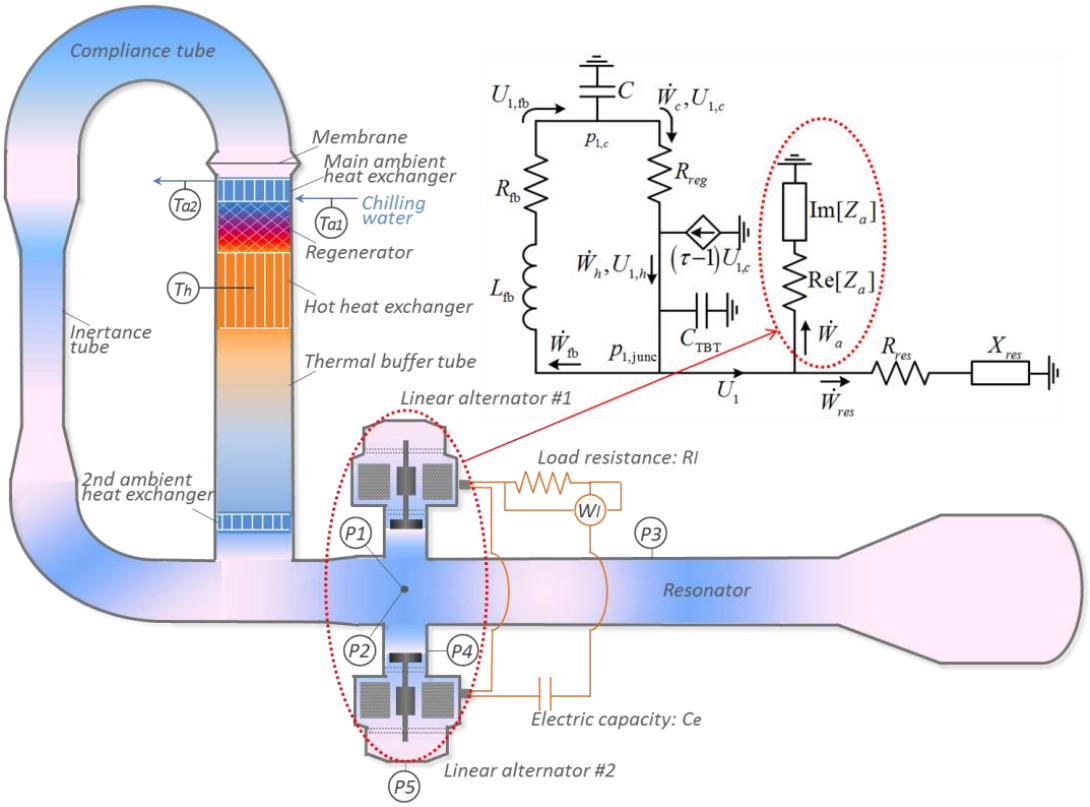

FIG. 1. Schematic diagram of traveling-wave thermoacoustic electric generator and the equivalent electric circuit network. *P1* denotes the location of a piezoresistive pressure sensor, and *P2*-*P5* denote that of piezoelectric pressure sensors. Heating temperature T_h, temperatures of the inlet T_{a1} and outlet T_{a2} of chilling water were measured by K-type thermocouples. The coils of the linear alternators are connected in series with a variable electric R-C load to extract electric power. Electric power W_l was measured by a power meter.

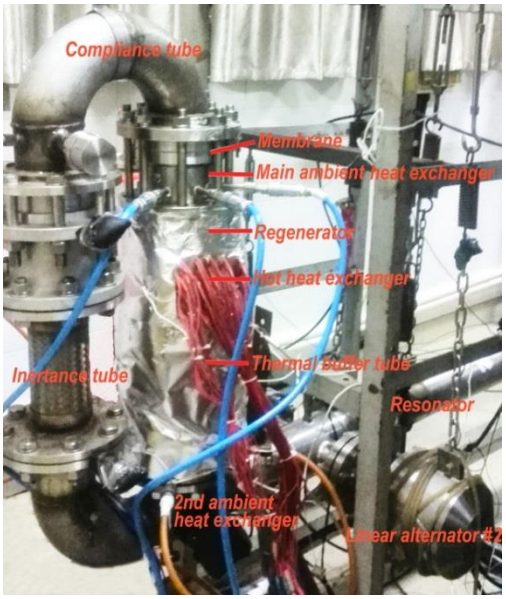

FIG. 2. Photograph of traveling-wave thermoacoustic electric generator. Note that only a part of the resonator is illustrated here. Linear alternator #1 was at the other side of the engine.

where thermoacoustic energy conversion occurs. The appropriate phase relation in the regenerator, i.e. zero phase difference between pressure and velocity, is achieved by the acoustic network formed by the tubes, including the compliance tube, inertance tube and resonator. The jet streaming in the thermal buffer tube is suppressed by using several layers of mesh screen as the flow straighter. The main dimensions of the TWTE can be found in Refs. [16, 31, 32], which are also given in TABLE 1. The parameters of the two LAs are listed in TABLE 2. The photograph of the experimental TWTEG is illustrated in FIG. 2. In the experiments, the electric power was measured by a power meter with an accuracy of 0.1%. The heating power was supplied by electric heaters, the power of which was measured by power meters with accuracies of 0.5%. The mean pressure was measured by a piezoresistive pressure sensor with an accuracy of 0.3%, while the high-frequency pressure oscillations were measured by piezoelectric pressure sensors PCB102B15 with accuracies of 1%.

The LAs and the gas resonators can be both represented by a resistance and a reactance. The acoustic resonance of the system is mainly determined by the compliance C above the main ambient heat exchanger and the inertance X_{res} of the gas resonator. When a large temperature gradient is established in the regenerator, self-excited acoustic oscillation occurs and acoustic power is amplified through the feedback network formed by the thermoacoustic torus. The net acoustic power flowing out of the torus partly goes into the LAs to generate electricity, and the rest goes into the resonator resulting in useless dissipations. The net acoustic power output of the torus and its distribution are determined by the acoustic impedances of the gas resonator and the LAs. Undoubtedly, appropriate modulations of the impedances to achieve a good matching of acoustic impedances are of great importance to improving the efficiency and power output.

TABLE 1. Main parameters of traveling-wave thermoacoustic engine.

Component	Diameter×Length (m)	Details
Main ambient heat exchanger	0.09×0.056	Shell-tube type, tube number 301, i.d. 2 mm
Regenerator	0.09×0.074	Stainless steel screen mesh, #120
Hot heat exchanger	0.09×0.12	Fin type, fin gap 1 mm, fin thickness 0.5 mm
Thermal buffer tube	0.1×0.291	/
2nd ambient heat exchanger	0.1×0.02	Shell-tube type, tube number 199, i.d. 3 mm
Inertance tube	0.076×0.28	/
Compliance tube	0.1×0.6767	/
Resonator	0.1×2.3	/

TABLE 2. Parameters of linear alternators.

Parameters	#1	#2
Force factor Bl (N/A)	90	90
Winding inductance L_e (mH)	268	263.4
Winding resistance r_e (Ω)	3.58	3.56
Mechanical stiffness K (N/m)	189235	188844
Mechanical resistance R_m (Ns/m)	5	2
Moving mass M (kg)	1.097	1.079
Piston area A (cm^2)	19.635	19.635
Back volume V_b (L)	1.63	1.63

The commonly used method in designing and optimizing a thermoacoustic system is to study the system as a whole by just using a complete model. However, if such method is routinely adopted for a TWTEG, it would obscure important information about the respective optimal operating conditions for the TWTE and the LAs, as they actually work individually to some extent, and meantime are coupled together in the integrated system [33]. As a result, effective acoustical matching between the TWTE and the LAs and the approaches for further improvements would be difficult to be realized. To clearly reveal the impedance coupling mechanism and make it easy to modulate the acoustic characteristics of the TWTEG, the TWTE and LAs are first decoupled and analyzed separately in the present study.

2.2 Model description

The calculations of the variations of the output acoustic power and thermal-to-acoustic efficiency of the TWTE with respect to the acoustic impedances of the load is based on linear thermoacoustic theory, which was first proposed by Rott [34] and then extended by Xiao [35-37] and Swift [38]. The main assumptions made for the thermoacoustic model are listed as follows:

- Time-dependent parameters, including pressure, velocity, volume flow, temperature and density, are composed of mean terms and time-dependent oscillating terms. All the time-dependent parameters are simple harmonic.
- Gas displacement amplitude is much smaller than the geometric dimensions in the direction that sound propagates.
- TWTE is treated as a one-dimension system.
- TWTE is assumed to be operated in a steady state.
- TWTE is operated in linear acoustics region so that nonlinear effects are ignored.
- Streaming caused by flow separations and thermal buoyancy, etc. is ignored.
- In turbulent flow region, the oscillatory flow is described by the Moody friction factor at each instant of time during the oscillatory flow, independent of the past history of the flow.
- Heat exchangers are assumed to be at uniform temperatures.

The frequency-domain momentum, continuity and energy equations of various components and flow channels in a thermoacoustic engine are expressed as follows [38],

$$\frac{dp_1}{dx} = -\frac{j\omega\rho_m}{1-f_\nu}\frac{U_1}{A}, \tag{1}$$

$$\frac{dU_1}{dx} = -\frac{j\omega A}{\gamma p_m}\left[1+(\gamma-1)f_\kappa\right]p_1 + \frac{f_\kappa - f_\nu}{(1-f_\nu)(1-\mathrm{Pr})}\frac{U_1}{T_m}\frac{dT_m}{dx}, \tag{2}$$

$$\frac{dT_m}{dx} = \frac{H - \frac{1}{2}\mathrm{Re}\left[p_1\tilde{U}_1\left(1-\frac{f_\kappa-\tilde{f}_\nu}{(1+\mathrm{Pr})(1-\tilde{f}_\nu)}\right)\right]}{\frac{\rho_m c_p|U_1|^2}{2A\omega(1-\mathrm{Pr}^2)|1-f_\nu|^2}\mathrm{Im}\left[f_\kappa+\mathrm{Pr}\,\tilde{f}_\nu\right]-(Ak+A_s k_s)}, \tag{3}$$

where p_1, U_1, T_m, and H are complex pressure amplitude, complex volume flow rate amplitude, mean temperature of working gas, and total energy flow, respectively; ω, γ, Pr, c_p and p_m represent angular frequency, specific heat ratio, Prandtl number, heat capacity and mean pressure, respectively;

f_κ and f_ν are thermal and viscous functions; k and k_s are thermal conductivities of gas and solid; A, A_s and x denote cross-sectional area for gas flow, solid cross-sectional area and coordinate along sound-propagation direction. Numerical solutions of the above equations can be obtained by adopting the widely used thermoacoustic software DeltaEC [9, 13, 21, 39, 40] developed by Los Alamos National Laboratory.

Ignoring the small differences between the parameters of the two LAs, the controlling equations for the voltage, force, and back volume of a LA can be expressed as follows respectively [38, 41],

$$Bl \cdot v_1 = I_1 \cdot \left(R_l/2 + r_e + j\omega L_e - j\frac{1}{2\omega C_e} \right), \tag{4}$$

$$\left(p_1 - p_{1,b}\right)A = Bl \cdot I_1 + R_m v_1 + \frac{K}{j\omega} v_1 + j\omega M v_1, \tag{5}$$

$$v_1 A = \frac{j\omega V_b}{\gamma p_m} p_{1,b}, \tag{6}$$

where v_1, I_1, p_1, $p_{1,b}$ are amplitudes of velocity, current, driving pressure, and pressure in the back volume of LAs.

In thermoacoustics, the acoustic impedance Z_a is defined as,

$$Z_a = \frac{p_1}{U_1} = \mathrm{Re}\left[\frac{p_1}{U_1}\right] + j\,\mathrm{Im}\left[\frac{p_1}{U_1}\right] = \frac{|p_1|}{|U_1|}\cos\theta_{p-U} + j\frac{|p_1|}{|U_1|}\sin\theta_{p-U}, \tag{7}$$

where || means the magnitude of a complex variable, and θ_{p-U} denotes the phase difference between pressure and volume flow. The real part of the acoustic impedance represents the acoustic resistance, which is a dissipative term in acoustics. The imaginary part stands for the acoustic reactance, i.e. acoustic inertance or acoustic compliance, which is an energy storage term.

By solving the Eqs. (4)-(6), the acoustic impedance Z_a of the two LAs, which are electrically connected in series, can be expressed by the basic parameters of LAs [38],

$$Z_a = \frac{1}{2A^2}\left[\left(R_m + \frac{R_e Bl^2}{R_e^{\,2} + X_e^{\,2}}\right) + j\left(X_m - \frac{X_e Bl^2}{R_e^{\,2} + X_e^{\,2}}\right)\right], \tag{8}$$

where $X_m = \omega M - \left(K + \gamma p_m A^2/V_b\right)/\omega$ is mechanical reactance, and $R_e = R_l/2 + r_e$ and $X_e = \omega L_e - 1/2\omega C_e$ are electrical resistance and reactance. The acoustic-to-electric efficiency of the LAs can be further derived,

$$\eta_{a-e} = \frac{W_l}{W_a} = \frac{Bl^2 R_l}{Bl^2 R_e + 2R_m\left(R_e^{\,2} + X_e^{\,2}\right)}. \tag{9}$$

With the above two equations, the dependences of the acoustic-to-electric efficiency on the acoustic impedance of the LAs can be obtained, and the methods for the modulation of the acoustic impedance can be analyzed. In the simulations, the LAs are modeled by the IESPEAKER component in DeltaEC program, and are combined with other components of the TWTE.

2.3 Acoustic impedance requirements of TWTE

The calculated acoustic impedance characteristics of the TWTE are shown in FIG. 3(a). The main ambient heat exchanger and the hot heat exchanger of the TWTE are fixed at 13 °C and 650 °C respectively, and the working fluid is helium of 3.16 MPa, which coincides with the working conditions in the experiments.

As shown, the acoustic power output W_a at the position where the LAs are connected and the corresponding thermal-to-acoustic efficiency $\eta_{t\text{-}a}$ of the TWTE have strong dependences on the acoustic impedance Z_a of the acoustic load. Both W_a and $\eta_{t\text{-}a}$ can reach their maximums at a specific real part of acoustic impedance Z_a, i.e. acoustic resistance Re[Z_a]. The optimal Re[Z_a] for the output acoustic power W_a at different acoustic reactances Im[Z_a] are all within the range of 1×10^7~3×10^7 Pa·s/m^3, while those for the efficiency $\eta_{t\text{-}a}$ are a little smaller, i.e. 5×10^6~2×10^7 Pa·s/m^3. For example, when acoustic reactance Im[Z_a] is fixed at zero which means the load is a pure acoustic resistance, the output acoustic power reaches the maximum of 837 W at Re[Z_a]=1.8×10^7 Pa·s/m^3, while the thermal-to-acoustic efficiency gets the maximum of 0.31 at Re[Z_a]=9×10^6 Pa·s/m^3. It indicates that the output acoustic power and the efficiency can not achieve their maximums at the same acoustic resistance, and compromises should be made between them when modulating the acoustic impedance of the LAs to couple with the thermoacoustic engine.

Furthermore, the acoustic reactance Im[Z_a] also has a strong influence on the output performance. The obtained maximum acoustic power and efficiency are the largest when the acoustic reactance Im[Z_a] equals zero, which indicates that it's beneficial to the output performance of the TWTE when

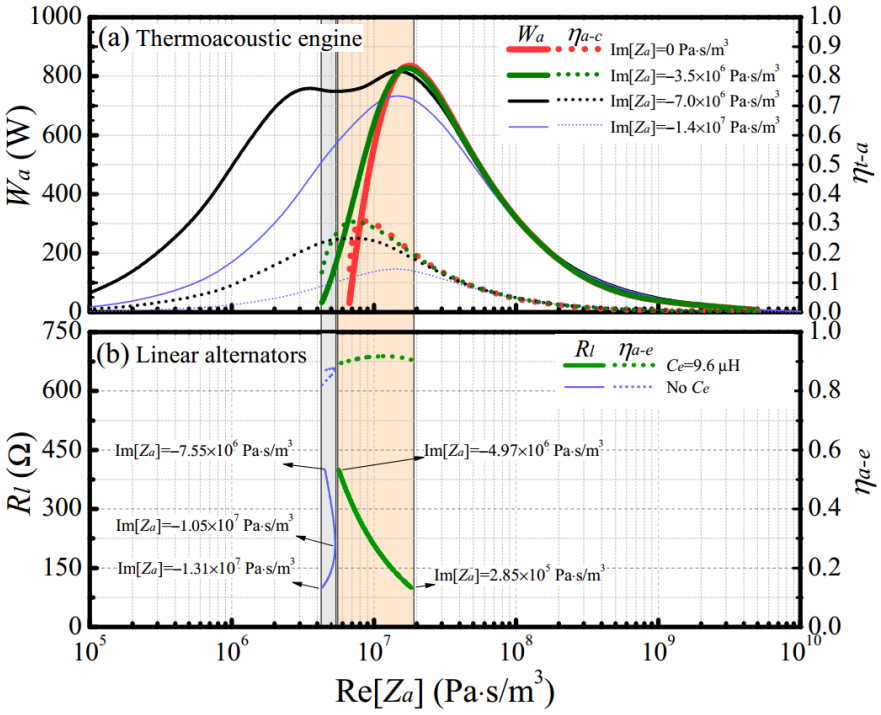

FIG. 3. Acoustic impedance characteristics of thermoacoustic engine and linear alternators: (a) Acoustic power output W_a and thermal-to-acoustic efficiency $\eta_{t\text{-}a}$ versus load acoustic impedance Z_a for thermoacoustic engine; (b) Load resistance R_l and acoustic-to-electric efficiency $\eta_{a\text{-}e}$ versus load acoustic impedance Z_a for linear alternators.

the acoustic load is a pure acoustic resistance. When Im[Z_a] is zero, both the acoustic power and the efficiency increase first slowly and later rapidly when decreasing the acoustic resistance Re[Z_a] to the optimal values, and then decrease sharply if Re[Z_a] is further decreased. When the acoustic resistance Re[Z_a] is less than 6.5×10^6 Pa·s/m^3, the acoustic power and the efficiency approach to zero, which indicates that the TWTE fails to work below this impedance. When the acoustic reactance Im[Z_a] of the load is -3.5×10^6 Pa·s/m^3, the range of the acoustic resistance Re[Z_a] in which the TWTE gets a relatively good performance becomes wider and the peak values of the acoustic power and efficiency are approximately the same as that with Im[Z_a]=0, as shown by the green solid and dash lines in FIG. 3(a). This means that it will be more convenient to modulate the acoustic impedance of the LAs at this acoustic reactance. When Im[Z_a]=-7×10^6 Pa·s/m^3, the optimal ranges of Re[Z_a] are even wider. However, both the acoustic power and efficiency get lower, especially the efficiency. When the acoustic load has a large capacitive reactance, the output performance, especially the thermal-to-acoustic efficiency of the TWTE, is remarkablely degraded, as shown by the lines of Im[Z_a]=-1.40×10^7 Pa·s/m^3.

In brief, it will be beneficial for the performance of the TWTE to set the magnitude of the imaginary part of the load acoustic impedance at a relatively small value, i.e. the order of 10^6 Pa·s/m^3 or even smaller. At this Im[Z_a], the optimal range of the real part of the load acoustic impedance for a large acoustic power output should be around 1×10^7~2×10^7 Pa·s/m^3, and that for a high thermal-to-acoustic efficiency is around 6×10^6~1×10^7 Pa·s/m^3.

2.4 Acoustic impedance modulation of LAs

According to the above analysis of the acoustic impedance requirements for the powerful and efficient operation of the TWTE, the magnitude of the imaginary part of acoustic impedance of the LAs, which is the acoustic load for the TWTE, should be very small. Therefore, the mechanical and electrical reactances X_m and X_e should be modulated to be both near zero, according to the expression of the acoustic impedance of LAs in Eq. (8). Besides, Eq. (8) also shows that the acoustic impedance Z_a of the given LAs can be modulated by adjusting the working frequency f, load resistance R_l, and electrical capacitance C_e.

The magnitude of the difference between the resonance frequencies of the TWTE and the LAs determines the magnitude of the mechanical reactance X_m for the given LAs, and further influences the impedance matching between them. The working frequency of the combined system is mainly determined by the dimensions of gas resonator and torus, and is adjusted to be about 65.5 Hz by changing the length of the gas resonator in the experiments. The resonance frequencies of the two LAs are about 68.7 Hz at 3.16 MPa. It indicates a near mechanical resonant state would achieve when the TWTE and LAs are connected together.

The effects of the load resistance R_l and electrical capacitance C_e on the acoustic impedance and acoustic-to-electric efficiency $\eta_{a\text{-}e}$ are given in FIG. 3(b). For the convenience of comparing the acoustic impedance characteristics between the TWTE and the LAs, the real part of the acoustic impedance of the LAs Re[Z_a] are set as the horizontal axis, though it is a dependent variable of R_l. If no external electric capacitance C_e is connected in the electric circuit, the electric reactance X_e is $2\omega L_e$. As shown, when the load resistance R_l is adjusted in the range from 100 Ω to 200 Ω, the corresponding

imaginary part of the acoustic impedance Im[Z_a] is far away from zero, i.e. in the range of -1.05×10^7~-1.31×10^7 Pa·s/m^3. According to Eq. (8), the real part of acoustic impedance Re[Z_a] is smaller when the electric reactance X_e is $2\omega L_e$ rather than zero. FIG. 3(b) shows that Re[Z_a] can only be modulated in a very narrow range of small values, i.e. from 4.32×10^6 Pa·s/m^3 to 5.32×10^6 Pa·s/m^3. Comparing the impedances of the LAs to the impedances of TWTE shown by the blue lines in FIG. 3(a), the output acoustic power and the thermal-to-acoustic efficiency of the TWTE are both relatively low when no electric capacitance C_e is connected. Moreover, the acoustic-to-electric efficiency $\eta_{a\text{-}e}$ of the LAs at this impedance is also limited, as shown by the blue dash line in FIG. 3(b). Though Im[Z_a] changes from -1.05×10^7 Pa·s/m^3 to -7.55×10^6 Pa·s/m^3 when the load resistance R_l is further increased from 200 Ω to 400 Ω, Re[Z_a] is still in the same small narrow range as that in R_l=100~200 Ω, and the corresponding acoustic power output and thermal-to-acoustic efficiency of the TWTE at these acoustic impedance conditions are still very limited, especially for the efficiency. Therefore, an acoustic impedance with an imaginary part far away from zero is not a suitable impedance condition for the efficient operations of both the LAs and the TE, which has also been experimentally proved by our previous studies [16].

In order to reduce the magnitude of the imaginary part of acoustic impedance Im[Z_a], an appropriate electric capacitance C_e can be connected in the circuit to offset the large inductive reactance of the LAs. Fortunately, the real part of the acoustic impedance Re[Z_a] is also increased if X_e is reduced. When C_e=9.6 μH, the imaginary part of acoustic impedance Im[Z_a] is modulated to be around -4.97×10^6~2.85×10^5 Pa·s/m^3 by adjusting the load resistance from 400 Ω to 100 Ω, which is much smaller compared to that when no C_e is connected. In the meanwhile, the real part of acoustic impedance can be increased and extended from 5.64×10^6 Pa·s/m^3 to 1.83×10^7 Pa·s/m^3, as shown by the green solid line in FIG. 3(b), perfectly covering the optimal impedances for both the output acoustic power and efficiency of the TWTE at the corresponding Im[Z_a]. Besides, the acoustic-to-electric efficiency of LAs is also remarkably increased compared to that when no C_e is connected. The above analysis shows that both the TWTE and LAs can both achieve their high performance points at this acoustic impedance, and will be well matched.

3. Experimental results

Based on the above analysis of impedance matching conducted by using a decoupling method, an integrated model of the TWTEG was then built, and an experimental system was further assembled, as shown in FIGs. 1 and 2. The coils of the LAs were connected in series with a variable load resistance R_l and a capacitance C_e of 9.6 μF to modulate both the real and imaginary parts of the acoustic impedance to the optimal ranges. Due to the restrictions of the allowable voltage and current of the LAs, the load resistance R_l was only adjusted from 100 Ω to 180 Ω when the heating temperature was 650 ℃ in the experiments. As a result, according to the calculation of the integrated model, the real part of acoustic impedance Re[Z_a] ranges from 1.86×10^7 Pa·s/m^3 to 1.14×10^7 Pa·s/m^3, which does not completely cover but is already quite near the optimal range for the output acoustic power and efficiency of the TWTE. Furthermore, the imaginary part of acoustic impedance Im[Z_a] of the LAs can be modulated from a large absolute value to a much smaller one after the capacitance C_e is added, i.e. from -1.31×10^7~1.09×10^7 Pa·s/m^3 to only 6.10×10^5~-3.25×10^6 Pa·s/m^3.

The experimental and calculated electric powers W_l of the integrated TWTEG are given in FIG. 4. As shown in FIG. 4(a), the calculated relationship between the electric power W_l and the load resistance R_l agrees well with the experimental results when the heating temperature are 650 °C and 600 °C respectively. The calculated pressure amplitudes, piston displacement, and working frequency agree well with the experimental data as well, as shown in FIGs. 5-7 respectively. The good agreement between the calculations and experiments shows that the main operating characteristics of the TWTEG have been well captured by the model and theoretical analysis. When decreasing the load resistance, the pressure amplitudes inside the TWTEG increase, as illustrated in FIG. 5. This is due to the lower dissipative mechanism caused by the lower load resistance. The piston displacement is positively related to the pressure amplitude and the load resistance [16]. Under the synergistic effect of the increasing pressure amplitude and the decreasing load resistance, the piston displacement decreases when decreasing the load resistance, as shown in FIG. 6. The generated electric power is approximately positive with the load resistance and the square of the pressure amplitude [16]. Larger pressure amplitudes provide stronger driving forces on the LAs. Whereas, a smaller load resistance has a negative effect on the electric power. Therefore, some optimal point would be achieved when decreasing the load resistance.

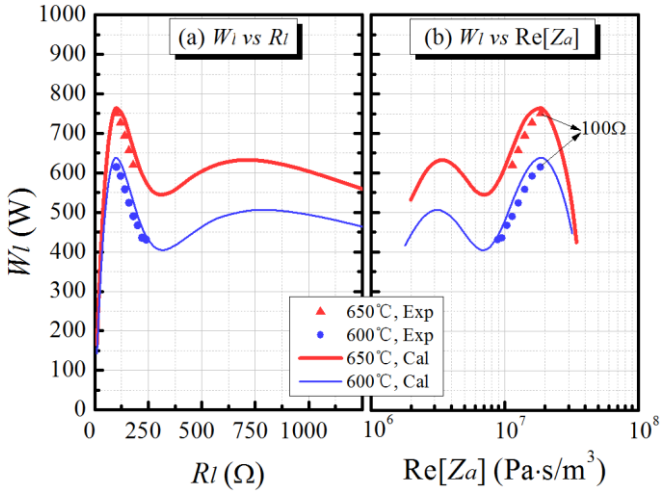

FIG. 4. Electric power W_l of traveling-wave thermoacoustic electric generator versus load resistance R_l and real part of acoustic impedance Re[Z_a], respectively.

To clearly reveal the mechanisms of the acoustic matching inside the TWTEG, the same data of the electric power in FIG. 4(a) are illustrated in terms of the real part of acoustic impedance Re[Z_a] in FIG. 4(b), which shows a good agreement too. The corresponding real part of acoustic impedance Re[Z_a] of the tested electric power in the experiments are extrapolated by using the LAs' model in consideration of the well validated integrated model of the TWTEG. When the load resistance R_l is 100 Ω, the electric power in the experiment reaches the maximum of 750.4 W when the heating temperature is 650 °C. According to the calculation, the electric power at this load resistance can reach its maximum of 765.8 W. Increasing the load resistance leads to the decrease of electric power in both the experiments and the calculations, as shown in FIG. 4(a). The variation trends aforementioned can be

explained by FIG. 4(b) and FIG. 3. When the load resistance R_l is 100 Ω, the imaginary part of acoustic impedance Im[Z_a] of the LAs is only 6.10×10^5 Pa·s/m^3, which is so small that the output characteristics

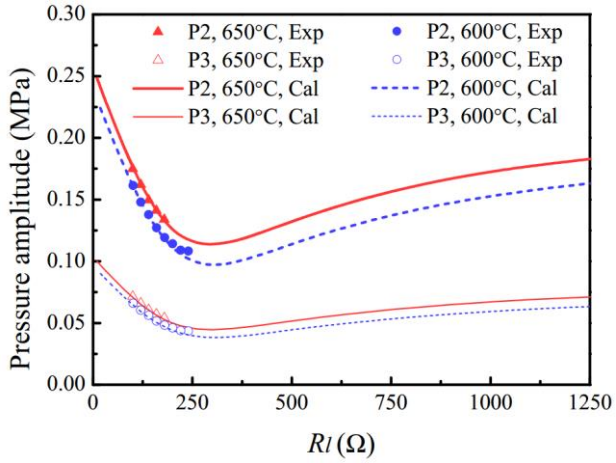

FIG. 5. Pressure amplitudes of P2 and P3 in traveling-wave thermoacoustic electric generator versus load resistance R_l.

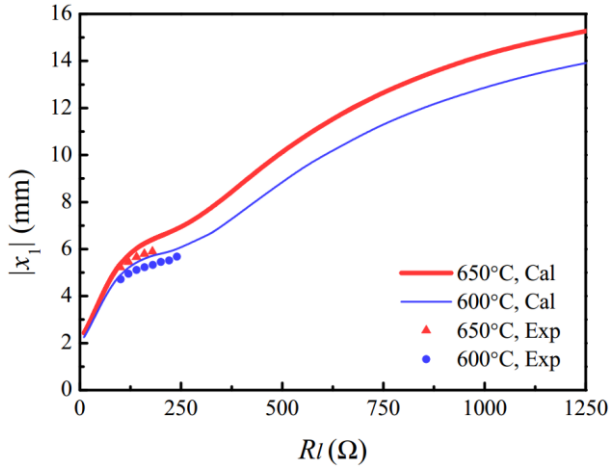

FIG. 6. Piston displacement of linear alternator #2 versus load resistance R_l.

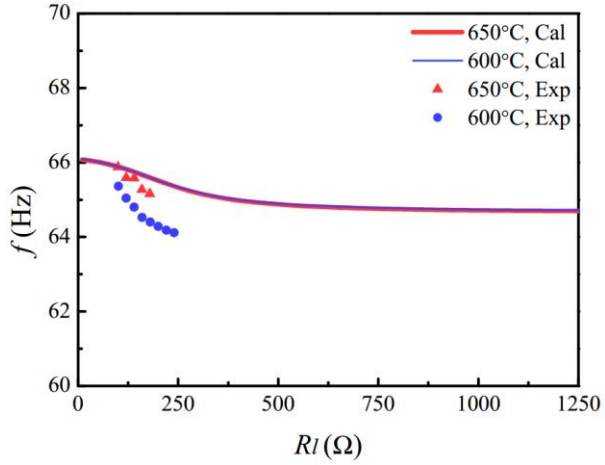

FIG. 7. Working frequency of traveling-wave thermoacoustic electric generator versus load resistance R_l.

of the TWTE is similar to that when Im[Z_a]=0. The real part of acoustic impedance Re[Z_a] of the Las is 1.86×10^7 Pa·s/m^3, which is approximately the optimal one required for the highest acoustic power output of the TWTE. As the acoustic-to-electric efficiency of the LAs stays almost constant at about 0.9, the integrated TWTEG system reaches its most powerful working point and thus gets the maximum electric power at 100 Ω. When increasing the load resistance to 180 Ω, the real part of acoustic impedance of the LAs decreases, as shown in FIG. 3(b). It weakens the output capacity of the TWTE, and further decreases the output electric power. If the load resistance is further increased from 180 Ω to 1400 Ω, the imaginary part of acoustic impedance is around -6.5×10^6 Pa·s/m^3, at which the acoustic power output characteristics of the TWTE are similar to that at Im[Z_a]=-7.0×10^6 Pa·s/m^3. Another peak of acoustic power output occurs. Therefore, the output electric power of the TWTEG shows another peak if load resistance is further increased. The variation trend of the electric power at 600 °C is similar, and up to 614.9 W electric power is achieved at this heating temperature.

The corresponding thermal-to-electric efficiencies of FIG. 4 are shown in FIG. 8. Different from the variation tendency of the electric power, the efficiency achieves the maximums at larger load resistances, whose real parts of acoustic impedances are smaller. It has been illustrated in FIG. 3(a) that smaller real part of acoustic impedance is required when a high efficiency is desired. The highest thermal-to-electric efficiency experimentally obtained is 0.163 while the calculated value is 0.24 at 160 Ω when the heating temperature is 650 °C. The deviations mainly result from the large heat losses from the hot heat exchanger, including the heat radiation and convection to the air and 2nd ambient heat exchanger through the thermal buffer tube, and the heat conduction through the pipes and regenerator filling. Besides, the backup heating elements that are installed at positions in the periphery of the hot heat exchanger have a much worse heat transfer performance, which influences the overall thermal-to-electric efficiency a lot. Last but not least, the loss from the membrane is not included yet. Comparing FIG. 4 and FIG. 8, even though the electric power can be remarkably increased by increasing the heating temperature from 600 °C to 650 °C, no significant improvement occurs for efficiency.

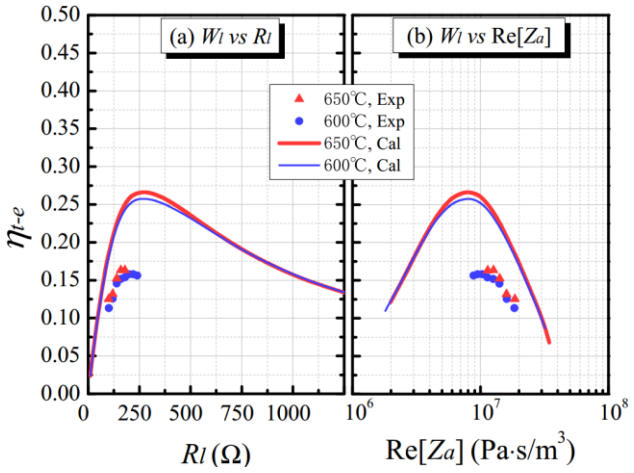

FIG. 8. Thermal-to-electric efficiency $\eta_{t\text{-}e}$ of traveling-wave thermoacoustic electric generator versus load resistance R_l and real part of acoustic impedance Re[Z_a], respectively.

It is well known that the operating pressure has a great influence on the power density and power output capacity of the TWTEG system. For safety reasons, the maximum working pressure adopted in the experiments is 3.16 MPa, which is well below those of the other thermoacoustic electric generation systems [17, 25, 28], let alone that of a common Stirling engine. If the working pressure is increased to 5.0 MPa, the performance of the same TWTEG is predicted in FIG. 9. The maximum electric power would exceed 1300 W with a thermal-to-electric efficiency of 0.20 at 73.4 Ω. The corresponding piston displacement is about 6.6 mm, which is just a little above the limit value of 6.5 mm of the LAs. If acoustic impedance matching, acoustic network, regenerators, and heat exchangers, etc. are further optimized, further improvements of the performance can be expected.

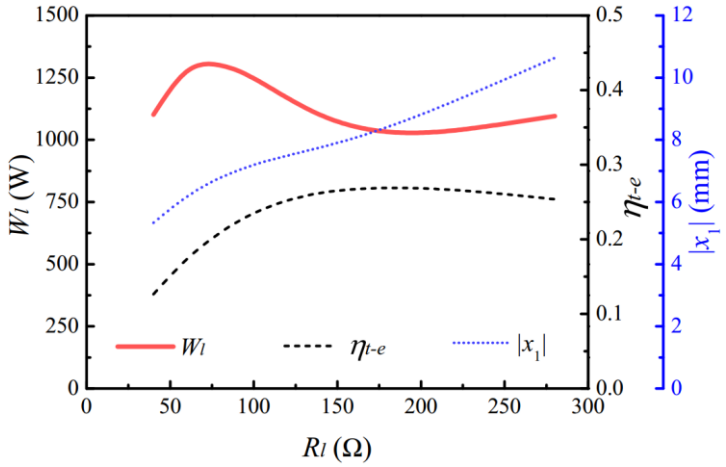

FIG. 9. Predicted performance of traveling-wave thermoacoustic electric generator working at 5.0 MPa.

4. Conclusion

An effective approach for acoustically matching a TWTEG has been proposed based on the comprehensive understanding of the acoustic characteristics of the TWTE and LAs. It would be instructive for the acoustic matching and designs of high-performance thermoacoustic electric generation systems. The main conclusions can be drawn as follows.

- The TWTE and LAs are first decoupled. The required acoustic impedances for efficient and powerful operations of the TWTE and LAs are then analyzed separately to clearly reveal the coupling mechanisms.
- It is beneficial for the output performance of the TWTE if the imaginary part of the load acoustic impedance is near zero. The optimal range of the real part for a large acoustic power output is around 1×10^7~2×10^7 Pa·s/m^3, while that for a high thermal-to-acoustic efficiency is about 6×10^6~1×10^7 Pa·s/m^3.
- When an electric capacitance of 9.6 μH is connected in the circuit of the LAs, the imaginary part of acoustic impedance is able to be modulated to be around the required range of the TWTE by adjusting the load resistance from 100 Ω to 400 Ω.
- An experimental TWTEG is then built and analyzed by modulating the working frequency, load resistance and electric reactance. A maximum electric power of 750.4 W and a highest thermal-to-electric efficiency of 0.163 were finally achieved when the acoustic impedance are well

matched. The predicted maximum electric power would exceed 1300 W with a thermal-to-electric efficiency of 0.20 if the mean pressure is increased to 5 MPa.

Acknowledgements

This work is financially supported by National Natural Science Foundation of China under contract No. 51476136. The authors acknowledge Dr. Yinong Wu from Shanghai Institute of Technical Physics and Dr. Wentai Qu from Zhejiang University for the kind help in the measurement systems.

References

[1] B. Oregan, M. Gratzel. A LOW-COST, HIGH-EFFICIENCY SOLAR-CELL BASED ON DYE-SENSITIZED COLLOIDAL TIO2 FILMS. Nature. 353 (1991) 737-40.

[2] C.J. Hsu, S.M. Sandoval, K.P. Wetzlar, G.P. Carman. Thermomagnetic conversion efficiencies for ferromagnetic materials. Journal of Applied Physics. 110 (2011) 123923.

[3] S. Saadon, O. Sidek. A review of vibration-based MEMS piezoelectric energy harvesters. Energy Conversion and Management. 52 (2011) 500-4.

[4] L.E. Bell. Cooling, heating, generating power, and recovering waste heat with thermoelectric systems. Science. 321 (2008) 1457-61.

[5] L. Rayleigh. THE EXPLANATION OF CERTAIN ACOUSTICAL PHENOMENA. Nature. 18 (1878) 319-21.

[6] S. Backhaus, G.W. Swift. A thermoacoustic Stirling heat engine. Nature. 399 (1999) 335-8.

[7] K. Wang, D.M. Sun, Y. Xu, J. Zou, X.B. Zhang, L.M. Qiu. Operating characteristics of thermoacoustic compression based on alternating to direct gas flow conversion. Energy. 75 (2014) 338-48.

[8] D.H. Li, Y.Y. Chen, E.C. Luo, Z.H. Wu. Study of a liquid-piston traveling-wave thermoacoustic heat engine with different working gases. Energy. 74 (2014) 158-63.

[9] Y. Zhao, Z. Yang, E.C. Luo, Y. Zhou. Travelling-wave thermoacoustic high-temperature heat pump for industrial waste heat recovery. Energy. 77 (2014) 397-402.

[10] D. Zhao, C. Ji, S. Li, J. Li. Thermodynamic measurement and analysis of dual-temperature thermoacoustic oscillations for energy harvesting application. Energy. 65 (2014) 517-26.

[11] A.A. Boroujerdi, M. Ziabasharhagh. Investigation of a high frequency pulse tube cryocooler driven by a standing wave thermoacoustic engine. Energy Conversion and Management. 86 (2014) 194-203.

[12] W. Chun, S.J. Oh, Y.J. Lee, S.H. Lim, R. Surathu, K. Chen. Acoustic waves generated by a TA (ThermoAcoustic) laser pair. Energy. 45 (2012) 541-5.

[13] H.F. Kang, P. Cheng, Z.B. Yu, H.F. Zheng. A two-stage traveling-wave thermoacoustic electric generator with loudspeakers as alternators. Applied Energy. 137 (2015) 9-17.

[14] K. Tang, T. Lei, T. Jin, X.G. Lin, Z.Z. Xu. A standing-wave thermoacoustic engine with gas-liquid coupling oscillation. Applied Physics Letters. 94 (2009) 254101.

[15] K. Wang, D. Sun, J. Zhang, N. Zhang, K. Luo, L. Qiu. Beating effect between a thermoacoustic source and its mechanical partner. Journal of Applied Physics. 118 (2015) 244907.

[16] D.M. Sun, K. Wang, X.J. Zhang, Y.N. Guo, Y. Xu, L.M. Qiu. A traveling-wave thermoacoustic electric generator with a variable electric R-C load. Applied Energy. 106 (2013) 377-82.

[17] Z.H. Wu, M. Man, E.C. Luo, W. Dai, Y. Zhou. Experimental investigation of a 500 W traveling-wave thermoacoustic electricity generator. Chinese Science Bulletin. 56 (2011) 1975-7.

[18] Z.H. Wu, G.Y. Yu, L.M. Zhang, W. Dai, E.C. Luo. Development of a 3 kW double-acting thermoacoustic Stirling electric generator. Applied Energy. 136 (2014) 866-72.

[19] K. Wang, D.M. Sun, J. Zhang, Y. Xu, J. Zou, K. Wu, et al. Operating characteristics and performance improvements of a 500 W traveling-wave thermoacoustic electric generator. Applied Energy. 160 (2015) 853-62.

[20] Y. Wang, Z. Li, Q. Li. A novel method for improving the performance of thermoacoustic electric generator without resonator. Energy Conversion and Management. 110 (2016) 135-41.

[21] Z.B. Yu, A.J. Jaworski, S. Backhaus. Travelling-wave thermoacoustic electricity generator using an ultra-compliant alternator for utilization of low-grade thermal energy. Applied Energy. 99 (2012) 135-45.
[22] C. Jensen, R. Raspet. Thermoacoustic power conversion using a piezoelectric transducer. The Journal of the Acoustical Society of America. 128 (2010) 98-103.
[23] A.A. Castrejon-Pita, G. Huelsz. Heat-to-electricity thermoacoustic-magnetohydrodynamic conversion. Applied Physics Letters. 90 (2007) 174110.
[24] C. Guthy, A.C.W. Van Neste, S. Mitra, S. Bhattacharjee, T. Thundat. Parametric energy conversion of thermoacoustic vibrations. Applied Physics Letters. 100 (2012) 203902.
[25] S. Backhaus, E. Tward, M. Petach. Traveling-wave thermoacoustic electric generator. Applied Physics Letters. 85 (2004) 1085-7.
[26] M. Petach, E. Tward, S. Backhaus. Design and Testing of A Thermal to Electric Power Converter Based On Thermoacoustic Technology. 2nd International Energy Conversion Engineering Conference. the American Institute of Aeronautics and Astronautics, Providence, Rhode Island, August 16-19, 2004.
[27] S.M. Oriti, N.A. Schifer. Recent Stirling Conversion Technology Developments and Operational Measurements at NASA Glenn Research Center. 7th International Energy Conversion and Engineering Conference (IECEC 2009), Denver, CO, USA, 2009.
[28] Z.H. Wu, L.M. Zhang, W. Dai, E.C. Luo. Investigation on a 1 kW traveling-wave thermoacoustic electrical generator. Applied Energy. 124 (2014) 140-7.
[29] T. Bi, Z. Wu, L. Zhang, G. Yu, E. Luo, W. Dai. Development of a 5 kW traveling-wave thermoacoustic electric generator. Applied Energy. (2015) (In Press).
[30] D.M. Sun, K. Wang, P. Lou, Y.T. Zhao, X.J. Zhang, L.M. Qiu. Investigation on working characteristics of Stirling-type thermoacoustic engine connected with linear alternator. Journal of Zhejiang University (Engineering Science). 47 (2013) 1457-62 (in Chinese)
[31] L.M. Qiu, D.M. Sun, W. Zhang, W.L. Yan, G.B. Chen. Investigation on traveling wave thermoacoustic heat engine with high pressure amplitude. Energy Conversion and Management. 46 (2005) 281-91.
[32] K. Wang, D.M. Sun, J. Zhang, J. Zou, K. Wu, L.M. Qiu, et al. Numerical simulation on onset characteristics of traveling-wave thermoacoustic engines based on a time-domain network model. International Journal of Thermal Sciences. 94 (2015) 61-71.
[33] H. Hatori, T. Biwa, T. Yazaki. How to build a loaded thermoacoustic engine. Journal of Applied Physics. 111 (2012) 074905.
[34] N. Rott. Thermoacoustics. Adv Appl Mech. 20 (1980) 135-75.
[35] J.H. Xiao. Thermoacoustic heat transportation and energy transformation. Part I: Formulation of the problem. Cryogenics. 35 (1995) 15-9.
[36] J.H. Xiao. Thermoacoustic heat transportation and energy transformation. Part II: Isothermal wall thermoacoustic effects. Cryogenics. 35 (1995) 21-6.
[37] J.H. Xiao. Thermoacoustic heat transportation and energy transformation. Part III: Adiabatic wall thermoacoustic effects. Cryogenics. 35 (1995) 27-9.
[38] G.W. Swift. Thermoacoustics: A unifying perspective for some engines and refrigerators. Acoustical Society of America, Sewickley, PA, USA, 2002.
[39] B. Ward, J. Clark, G.W. Swift. Design Environment for Low-amplitude Thermoacoustic Energy Conversion. Version 6.2. Users Guide.2008.
[40] S. Backhaus, G.W. Swift. A thermoacoustic-Stirling heat engine: Detailed study. The Journal of the Acoustical Society of America. 107 (2000) 3148-66.
[41] Z.H. Wu, E.C. Luo, W. Dai. Theoretical investigation on linear alternator in thermoacoustic power generation system. Taiyangneng Xuebao/Acta Energiae Solaris Sinica. 29 (2008) 493-7 (in Chinese).

Nomenclature

A Cross-sectional area of gas flow channels, piston area, m^2

A_s Cross-sectional area of solid

Bl Force factor, N/A

C Acoustic compliance, m^3/Pa

C_e Electrical capacitance, F

c_p Specific heat at constant pressure, J/(kg·K)

f Working frequency, Hz

f_κ Spatial averaged thermal function

f_ν Spatial averaged viscous function

H Total energy flow, W

I_1 Complex current, A

Im[] Imaginary part of a complex variable

j $\sqrt{-1}$

k Thermal conductivity of gas, W/(m·K)

K Mechanical stiffness, N/m

k_s Thermal conductivity of solid, W/(m·K)

L_e Winding inductance, H

M Moving mass, kg

p_1 Complex pressure amplitude, Pa

$p_{1,b}$ Complex pressure amplitude in back volume, Pa

p_m Mean pressure, Pa

Pr Prandtl number

r_e Winding resistance, Ω

R_e Electrical resistance, Ω

Re[] Real part of a complex variable

R_l Load resistance, Ω

R_m Mechanical resistance, N·s/m

T_m Temperature, K

U_1 Complex volume flow rate, m^3/s

v_1 Complex velocity of piston, m/s

V_b Back volume, L

x Coordinate along sound-propagation direction, m

x_1 Piston displacement, m

X_e Eletrical reactance, Ω

X_m Mechanical reactance, kg/s

X_{res} Acoustic reactance of gas resonator, $kg/m^4 \cdot s$

Z_a Acoustic impedance, $Pa \cdot s/m^3$

$\theta_{p\text{-}U}$ Phase difference between pressure and volume flow, rad

γ Specific heat ratio

ρ_{m} Density, kg/m^3

ω Angular frequency, rad/s

η_{a-e} Acoustic-to-electric efficiency of LA

η_{t-a} Thermal-to-Acoustic efficiency of TWTE

η_{t-e} Thermal-to- electric efficiency of TWTEG

Special symbols

| | Magnitude of complex variable

~ Complex conjugate